Multiple functional self-association interfaces in plant TIR domains

Xiaoxiao Zhang[a,b,1], Maud Bernoux[b,1,2], Adam R. Bentham[a,c,1], Toby E. Newman[d,e], Thomas Ve[a,f], Lachlan W. Casey[a], Tom M. Raaymakers[b,g], Jian Hu[b,h], Tristan I. Croll[i], Karl J. Schreiber[j], Brian J. Staskawicz[j,2], Peter A. Anderson[c], Kee Hoon Sohn[d,e], Simon J. Williams[a,k,2], Peter N. Dodds[b,2], and Bostjan Kobe[a,2]

[a]School of Chemistry and Molecular Biosciences, Australian Infectious Diseases Research Centre and Institute for Molecular Bioscience, University of Queensland, Brisbane, QLD 4072, Australia; [b]Agriculture and Food, Commonwealth Scientific and Industrial Research Organisation, Canberra, ACT 2601, Australia; [c]School of Biological Sciences, Faculty of Science and Engineering, Flinders University, Adelaide, SA 5001, Australia; [d]Department of Life Sciences, and School of Interdisciplinary Bioscience and Bioengineering, Pohang University of Science and Technology, Pohang, Gyeongbuk 790-784, Republic of Korea; [e]Bioprotection Research Centre, Institute of Agriculture and Environment, Massey University, Palmerston North 4442, New Zealand; [f]Institute for Glycomics, Griffith University, Southport, QLD 4222, Australia; [g]Department of Biology, Plant–Microbe Interactions, Utrecht University, 3584 CH Utrecht, The Netherlands; [h]College of Biological Sciences, China Agricultural University, Beijing 100094, People's Republic of China; [i]School of Biomedical Sciences, Queensland University of Technology, Brisbane, QLD 4001, Australia; [j]Department of Plant and Microbial Biology, University of California, Berkeley, CA 94720; and [k]Research School of Biology, College of Medicine, Biology, and Environment, Australian National University, Canberra, ACT 0200, Australia

Contributed by Brian J. Staskawicz, December 28, 2016 (sent for review November 29, 2016; reviewed by Blake C. Meyers and Ryohei Terauchi)

The self-association of Toll/interleukin-1 receptor/resistance protein (TIR) domains has been implicated in signaling in plant and animal immunity receptors. Structure-based studies identified different TIR-domain dimerization interfaces required for signaling of the plant nucleotide-binding oligomerization domain-like receptors (NLRs) L6 from flax and disease resistance protein RPS4 from *Arabidopsis*. Here we show that the crystal structure of the TIR domain from the *Arabidopsis* NLR suppressor of npr1-1, constitutive 1 (SNC1) contains both an L6-like interface involving helices αD and αE (DE interface) and an RPS4-like interface involving helices αA and αE (AE interface). Mutations in either the AE- or DE-interface region disrupt cell-death signaling activity of SNC1, L6, and RPS4 TIR domains and full-length L6 and RPS4. Self-association of L6 and RPS4 TIR domains is affected by mutations in either region, whereas only AE-interface mutations affect SNC1 TIR-domain self-association. We further show two similar interfaces in the crystal structure of the TIR domain from the *Arabidopsis* NLR recognition of *Peronospora parasitica* 1 (RPP1). These data demonstrate that both the AE and DE self-association interfaces are simultaneously required for self-association and cell-death signaling in diverse plant NLRs.

plant immunity | NLR | TIR domain | plant disease resistance | signaling by cooperative assembly formation

Plants have evolved a sophisticated innate immune system to detect pathogens, in which plant resistance (R) proteins recognize pathogen proteins (effectors) in a highly specific manner. This recognition leads to the effector-triggered immunity (ETI) response that often induces a localized cell death known as the hypersensitive response (1). Most R proteins belong to the nucleotide-binding oligomerization domain (NOD)-like receptor (NLR) family. NLRs are prevalent in the immune systems of plants and animals and provide resistance to a broad range of pathogens, including fungi, oomycetes, bacteria, viruses, and insects (2, 3). NLRs contain a central nucleotide-binding (NB) domain, often referred to as the nucleotide-binding adaptor shared by APAF-1, resistance proteins, and CED-4 (NB-ARC domain) (4) and a C-terminal leucine-rich repeat (LRR) domain. Plant NLRs can be further classified into two main subfamilies, depending on the presence of either a Toll/interleukin-1 receptor domain (TIR–NLR) or a coiled-coil domain (CC–NLR) at their N termini (5).

The CC and TIR domains of many plant NLRs can autonomously signal cell-death responses when expressed ectopically in planta, and mutations in these domains within full-length proteins also compromise signaling, suggesting that these domains are responsible for propagating the resistance signal after activation of the receptor (6–14). Self-association of both TIR (8, 9, 11, 15) and CC (10, 13, 16, 17) domains has been shown to be important for the signaling function. In animal NLRs, the formation of postactivation oligomeric complexes, such as the NLRC4/NAIP inflammasome or the APAF1 apoptosome, is important for bringing together N-terminal domains into a signaling platform (18–20), but there is yet little evidence for such signaling complexes in plants.

Several crystal structures of plant TIR domains have been reported (9, 11, 21–24). These structures reveal a similar overall structure, which consists of a flavodoxin-like fold containing a central parallel β-sheet surrounded by α-helices. This fold is shared with the TIR domains from animal innate immunity proteins, although plant TIR domains generally have an extended αD-helical region that is not found in the animal TIR domains. Whereas the overall structure of plant TIR domains is conserved, the identified self-association interfaces differ. The crystal structure of $L6^{TIR}$ revealed an interface predominantly formed by the αD- and αE-helices (termed here the DE interface) (9). Mutations in this interface disrupt $L6^{TIR}$ self-association and signaling activity (9). In the case of disease resistance protein RPS4 TIR domain ($RPS4^{TIR}$)

Significance

Toll/interleukin-1 receptor/resistance protein (TIR) domains are present in plant and animal innate immunity receptors and appear to play a scaffold function in defense signaling. In both systems, self-association of TIR domains is crucial for their function. In plants, the TIR domain is associated with intracellular immunity receptors, known as nucleotide-binding oligomerization domain-like receptors (NLRs). Previous studies from several plant NLRs have identified two distinct interfaces that are required for TIR:TIR dimerization in different NLRs. We show that the two interfaces previously identified are both important for self-association and defense signaling of multiple TIR–NLR proteins. Collectively, this work suggests that there is a common mechanism of TIR domain self-association in signaling across the TIR–NLR class of receptor proteins.

Author contributions: X.Z., M.B., A.R.B., T.V., L.W.C., B.J.S., K.H.S., S.J.W., P.N.D., and B.K. designed research; X.Z., M.B., A.R.B., T.E.N., L.W.C., T.M.R., J.H., K.H.S., S.J.W., and P.N.D. performed research; M.B., K.H.S., and P.N.D. contributed new reagents/analytic tools; X.Z., M.B., A.R.B., T.V., L.W.C., T.I.C., K.J.S., B.J.S., P.A.A., K.H.S., S.J.W., P.N.D., and B.K. analyzed data; and X.Z., M.B., A.R.B., L.W.C., K.H.S., S.J.W., P.N.D., and B.K. wrote the paper.

Reviewers: B.C.M., Donald Danforth Plant Science Center; and R.T., Iwate Biotechnology Research Center.

The authors declare no conflict of interest.

Data deposition: The protein structures and data used to derive these structures have been deposited in the Protein Data Bank, www.pdb.org [PDB ID codes 5TEB ($RPP1^{TIR}$) and 5TEC ($SNC1^{TIR}$)].

See Commentary on page 2445.

[1]X.Z., M.B., and A.R.B. contributed equally to this work.

[2]To whom correspondence may be addressed. Email: stask@berkeley.edu, maud.bernoux@csiro.au, simon.williams@anu.edu.au, peter.dodds@csiro.au, or b.kobe@uq.edu.au.

This article contains supporting information online at www.pnas.org/lookup/suppl/doi:10.1073/pnas.1621248114/-/DCSupplemental.

and disease resistance protein RRS1 TIR domain (RRS1^{TIR}), an interface involving the αA- and αE-helices (the AE interface) was observed in the crystal structures of both individual protein domains and of the RPS4^{TIR}:RRS1^{TIR} heterodimer (11). Dimerization of RPS4^{TIR}:RRS1^{TIR} and self-association of RPS4^{TIR} are dependent on the integrity of the AE interface, and mutations that disrupt this interface prevent both resistance signaling of the RPS4:RRS1 NLR pair and the autoactivity of RPS4^{TIR}.

The different dimerization interfaces in L6^{TIR} and RPS4^{TIR} raise the question of whether either or both of these interfaces have conserved roles in other TIR–NLRs. To address this question, we investigated the structure and function of TIR domains from several plant NLRs. We present the crystal structures of TIR domains from the *Arabidopsis* NLR proteins suppressor of npr1-1, constitutive 1 (SNC1) (25) and recognition of *Peronospora parasitica* 1 (RPP1) (26). The two structures reveal the presence of both DE- and AE-type interaction interfaces. Site-directed mutagenesis of SNC1, L6, and RPS4 reveals that both the AE- and DE-interaction surface regions can be simultaneously involved in self-association (L6 and RPS4) and are required for signaling of these TIR domains. These data imply that self-association through both the AE and DE interfaces plays a general role in TIR-domain signaling in plant immunity.

Results

The Crystal Structure of SNC1^{TIR} Reveals RPS4 and L6-Like Interfaces. We crystallized the TIR domain (residues 8–181) from the *Arabidopsis* NLR protein SNC1 (SNC1^{TIR}) (27) and determined the structure at 2.2-Å resolution (*SI Appendix*, Table S1). The fold features a four-stranded β-sheet (strands βA and βC–βE) surrounded by α-helices (αA–αE) (*SI Appendix*, Figs. S1 and S2*A*). No electron density was observed for the terminal residues (8–9 and 176–181) and residues 46–57 (corresponding to the βB-strand loop helix in L6^{TIR}; *SI Appendix*, Figs. S1 and S2*A*).

In the SNC1^{TIR} crystal, there are two prominent interfaces between molecules (Fig. 1*A*). These interfaces have striking similarities to the AE and DE interface that we previously observed in the structures of RPS4^{TIR} and L6^{TIR}, respectively (Fig. 1 *B* and *C*). Hyun et al. also observed the analogous interfaces in a recent report (24). The AE interface is formed by a symmetrical interaction involving the αA and αE helices (Fig. 1*D*) of the two molecules (hereafter designated molecules "A" and "B"), yielding a total buried surface area of ∼1,000 Å^2. The AE interface in SNC1^{TIR} contains the conserved SH (serine–histidine) motif (*SI Appendix*, Fig. S3 *A* and *B*), which is required for RPS4^{TIR} autoactivity and RPS4^{TIR}:RRS1^{TIR} dimerization and function of the full-length paired-NLR proteins (11). Side chains of the two histidines (H30$_A$ and H30$_B$, located in the center of opposing αA-helices) stack, with the neighboring serines (S29) forming hydrogen-bonding interactions with the backbone of A159 in the opposing αE-helices (Fig. 1*D*). The AE interface is further stabilized by a dense hydrogen-bonding network and electrostatic interactions between charged residues of the αA- and αE-helices that flank the SH motif, including interactions K33$_A$–E34$_B$ and E164$_B$, H30$_A$–E158$_B$, and E158$_A$–D25$_B$.

The DE interface in SNC1^{TIR} involves the αD$_1$- and αE-helices and the connecting loops and strands (molecules "A" and "C"). There are fewer hydrogen-bonding interactions in it, compared with the AE interface; however, several complementary hydrophobic residues are buried (Fig. 1*E* and *SI Appendix*, Fig. S2*B*). Residues within the βE-strand and αE-helices of the contacting molecules form hydrogen bonds (K154$_C$–G149$_A$ and Y150$_A$; K154$_A$–R153$_C$). E164$_A$ and E167$_A$ form salt bridges with K154$_C$ and K112$_C$, respectively. The DE interface also contains a cation–π interaction between the W155$_A$ aromatic ring and the R153$_C$ side chain (*SI Appendix*, Fig. S2*B*). The SNC1^{TIR} and L6^{TIR} DE interfaces involve similar surface regions (Fig. 1*C*), although after superimposition of one molecule in the pair, the second SNC1^{TIR} and L6^{TIR} molecules are rotated ∼21° relative to each other (Fig. 1*C*). Unlike L6^{TIR}, the αD$_3$-helix of SNC1^{TIR} does not contribute to the interactions with the neighboring molecule in the crystal lattice, and the interface in SNC1^{TIR} is slightly smaller than

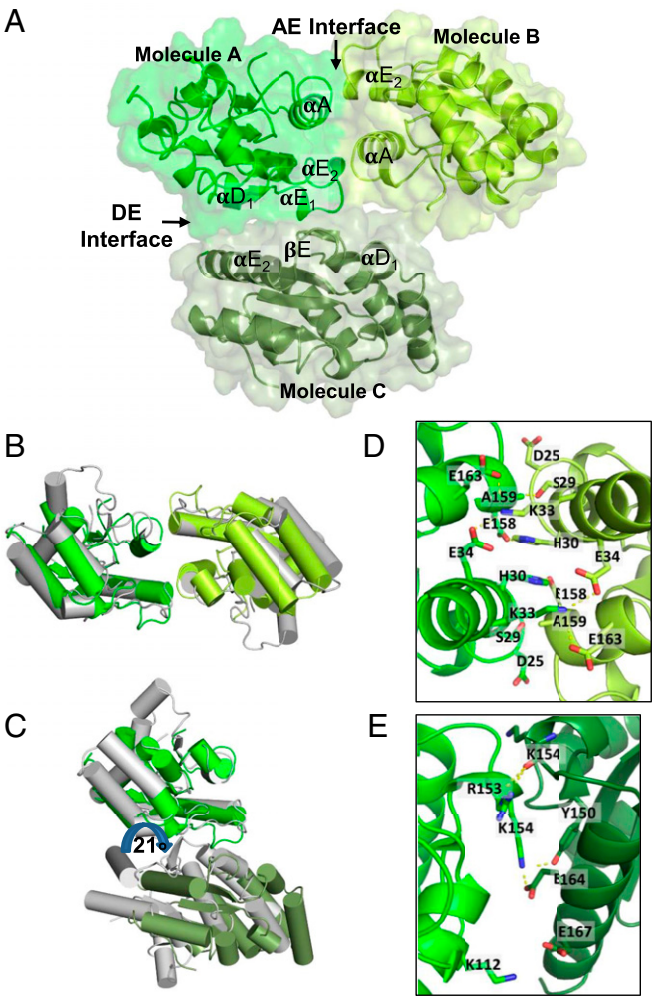

Fig. 1. The crystal structure of SNC1^{TIR} reveals two self-association interfaces. (*A*) SNC1^{TIR} crystal structure contains two major interfaces, involving predominantly αA and αE (AE) and αD and αE (DE) regions of the protein. The green and lime-colored SNC1^{TIR} molecules are observed in the asymmetric unit and interact through the AE interface; the green molecule also interacts with a crystallographic symmetry-related molecule (forest colored) through the DE interface. (*B*) Superposition of the SNC1^{TIR} (green and lime) and RPS4^{TIR} (gray) AE-interface dimers; one chain in the pair was used for superposition. (*C*) As in *B*, but showing the superposition of SNC1^{TIR} and L6^{TIR} (gray) DE-interface dimers; note the ∼21° rotation at the DE interface between the two structures. (*D*) Residues that contribute to the buried surface in the AE-interface interactions in SNC1^{TIR} are highlighted in stick representation. (*E*) As in *D*, showing the DE interface.

in L6^{TIR} (buried surface area 812 Å^2 for SNC1^{TIR} and 890 Å^2 for L6^{TIR}). Sequence analysis of plant TIR domains reveals that most of the coordinating residues involved in the DE interface in SNC1^{TIR} are not conserved (including K112, K154, and E164), with the exception of G149 (*SI Appendix*, Fig. S3 *C* and *D*), contrasting the conservation in the AE interface.

Self-Association of SNC1^{TIR} in Solution Is Disrupted by Mutations in the AE Interface. Reversible self-association in solution is observed for L6^{TIR} and RPS4^{TIR} (9, 11). We used size-exclusion chromatography (SEC) coupled to multiangle light scattering (MALS) to examine the ability of SNC1^{TIR} to self-associate in solution. By SEC-MALS, the average molecular mass of SNC1^{TIR} was higher than the theoretical molecular mass of a monomer (20.1 kDa) and increased with protein loading (Fig. 2*A*). Using the complementary technique small-angle X-ray scattering (SAXS), a similar concentration-dependent increase in average molecular

mass was observed (Fig. 2*B*). These data suggest that SNC1^{TIR} self-associates in solution in a concentration-dependent manner and is in a rapid equilibrium between monomeric and oligomeric (dimeric or higher-order) protein species.

L6^{TIR} and RPS4^{TIR} self-association in solution was shown to be dependent on the DE and AE interfaces, respectively (9, 11). To test whether these protein surfaces play a role in SNC1^{TIR} self-association, key residues involved in forming the two interfaces were mutated (to alanine or amino acid of opposite charge) and the mutant proteins tested using SEC-MALS. These residues include four in the AE interface (S29, H30, K33, and E163), and four in the DE interface (K112, Y150, K154, and E164). Recombinant proteins of all mutants, except Y150A, were successfully produced in *Escherichia coli*. With the exception of E163A, all mutants in the AE interface had average molecular masses close to the expected monomeric mass of SNC1^{TIR} (*SI Appendix*, Table S2 and Fig. S4*A*), and there was no concentration-dependent increase in the molecular mass of the H30A mutant when analyzed by SEC-MALS and SAXS (Fig. 2 *A* and *B*). Therefore, the S29A, H30A, and K33A mutations disrupt SNC1^{TIR} self-association in solution. The E163A mutant had a reduced molecular mass compared with the wild-type protein, suggesting this mutation had a weaker effect on SNC1^{TIR} self-association, probably due to its location at the periphery of the AE interface. By contrast, we could not detect an effect on self-association of mutants in the DE interface (K112A or E, K154A or E, and E164A or K) using SEC-MALS. These observations suggest that the AE interface contributes more than the DE interface to the self-association of the SNC1^{TIR} in solution.

SNC1^{TIR} Autoactivity Is Disrupted by Mutations in Either AE or DE Interfaces. To test the biological relevance of the AE and DE interfaces for SNC1^{TIR} function, we tested the effect of interface mutations on SNC1^{TIR} cell-death signaling. *Agrobacterium*-mediated transient expression of SNC1^{TIR} (residues 1–226) in *Nicotiana benthamiana* induced a visible chlorotic cell-death phenotype 5 d after infiltration. Expression of mutants in the AE interface, including S29A, H30A, and K33A, resulted in a much weaker cell-death response and a significantly reduced level of ion leakage compared with the wild-type protein (*SI Appendix*, Table S2 and Fig. 2 *C*–*F*). The E163A mutant, which showed modestly impaired self-association in solution, did not reduce the level of cell-death phenotype nor ion leakage, compared with the wild-type protein. Overall, these effects correlate well with the effects on self-association, suggesting that the integrity of the AE interface is required for both TIR domain self-association and signaling activity.

Amino acid substitutions of the DE-interface residues also affected SNC1^{TIR} autoactivity (*SI Appendix*, Table S2 and Fig. 2 *C*–*F*). The Y150A mutation, which is at the center of the SNC1^{TIR} DE interface, significantly disrupted autoactivity. Notably, L6^{TIR} has a tryptophan residue (W202) at the equivalent position (*SI Appendix*, Fig. S1) and its substitution with alanine abolished L6^{TIR} self-association in yeast and signaling activity in planta (9). Both K112E and K154E mutations in SNC1^{TIR} led to a reduced cell-death phenotype level, whereas alanine substitution of either residue did not, consistent

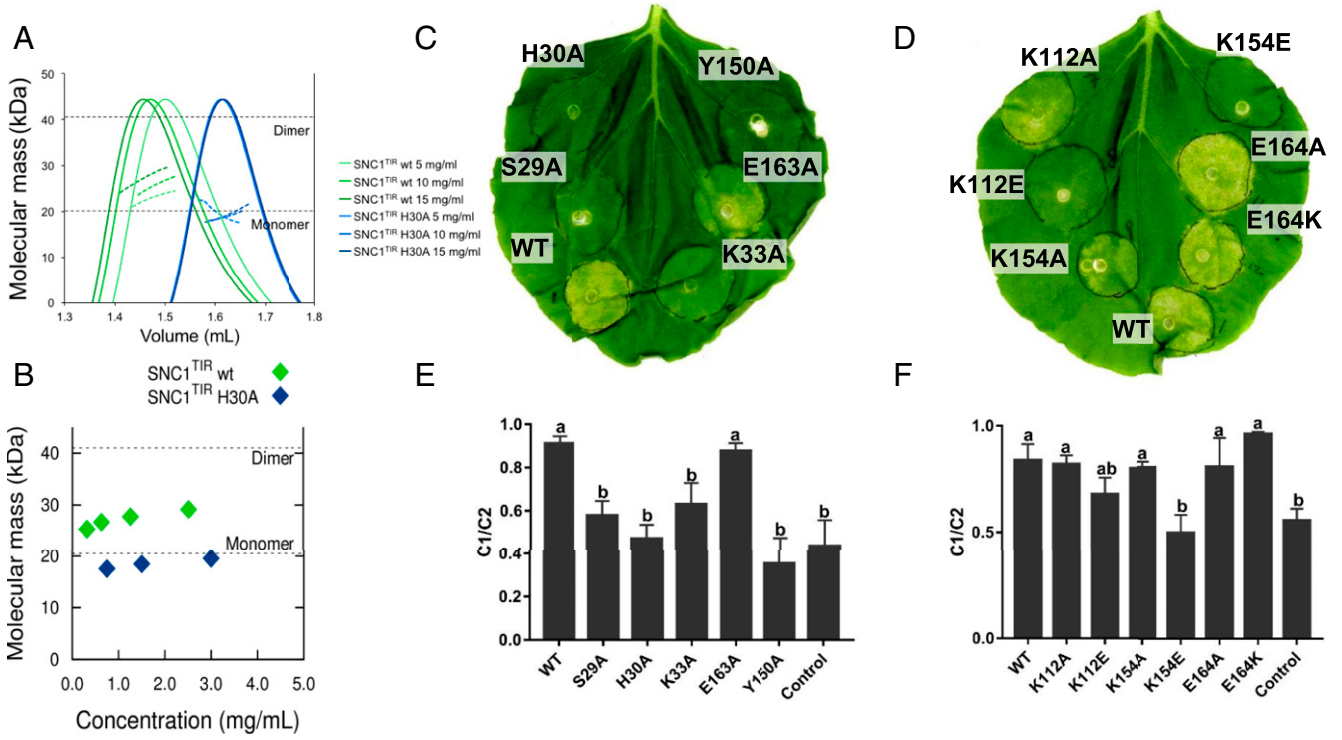

Fig. 2. SNC1^{TIR} self-association and signaling. (*A*) Solution properties of SNC1^{TIR} (WT, wild-type) and SNC1^{TIR} H30A analyzed by SEC-MALS. Green or blue peaks indicate the traces from the refractive index (RI) detector during SEC of SNC1^{TIR} or its H30A mutant, respectively. The lines under the peaks correspond to the average molecular mass distributions across the peak (using equivalent coloring). (*B*) Molecular masses calculated from SAXS data for SNC1^{TIR} (WT, wild-type; green diamonds) and SNC1^{TIR} H30A (blue diamonds), calculated from static samples at discrete concentrations between 3 and 0.25 mg/mL. Dotted lines indicate the theoretical monomeric and dimeric masses. (*C*–*F*) In planta mutational analysis of SNC1^{TIR}. (*C* and *D*) Autoactive phenotype of SNC1^{TIR} (residues 1–226; WT, wild-type) and the corresponding mutants upon *Agrobacterium*-mediated transient expression in *N. benthamiana* leaves. Each construct was coexpressed with the virus-encoded suppressor of gene silencing P19 (33). Photos were taken 5 d after infiltration. (*E* and *F*) Ion-leakage measurement of the infiltrated leaves as shown in *C* and *D*. Each construct was expressed in independent leaves. Leaf disk samples were collected 2 d after infiltration and incubated in Milli-Q water. C1 corresponds to the ions released in solution 24 h after sampling. C2 corresponds to the total ion contents in the sample (see *SI Appendix, Methods* for details). Ion leakage was calculated as C1/C2 ratio. *N. benthamiana* leaves expressing P19 only were used as control. Error bars show SE of means. Statistical differences, calculated by one-way ANOVA and multiple comparison with the control, are indicated by letters.

with electrostatic interactions through the charged side chains. By contrast, neither A nor K substitutions of the E164 residue affected cell-death development. All mutants were detected by immunoblotting and had similar protein expression levels (*SI Appendix*, Fig. S5*A*), indicating the abolition of autoactivity was not due to protein-expression differences.

Residues in the AE Interface Contribute to L6^{TIR} Self-Association and Autoactivity. We previously showed that the DE interface was involved in L6^{TIR} self-association and autoactivity (9), but the AE interface was not observed in the L6^{TIR} crystal structure. To test whether the AE interface is relevant for L6^{TIR} function, we first modeled this potential interface by superimposing the L6^{TIR} molecules onto the RPS4^{TIR} AE-interface dimer (*SI Appendix*, Fig. S6*A*). The L6^{TIR} has a phenylalanine (F79) at the position equivalent to the conserved histidine that forms the core of the AE interfaces in both RPS4^{TIR} and SNC1^{TIR} (Fig. 1*D* and *SI Appendix*, Fig. S6*A*). The equivalent residue is a phenylalanine in AtTIR, where it is involved in an AE interface in a stacking arrangement analogous to the histidine residues in SNC1^{TIR} and RPS4^{TIR} (11, 22). An aspartate residue precedes F79 in L6^{TIR}, occupying the position of the conserved serine in RPS4^{TIR}. The modeling also indicates that residues E74 and Q82 in the αA-helix, and K209 in the αE-helix could form hydrogen bonds in a potential AE-interface interaction in L6^{TIR}.

To test whether the AE interface is involved in L6^{TIR} function, we examined the effect of amino acid substitutions in this interface on its self-association. Mutations of residues F79A and K209E disrupted L6^{TIR} self-association in yeast-two-hybrid (Y2H) assays, whereas the E74K mutation did not (Fig. 3*A*). Protein expression of the BD fusion of the F79A mutant was detected at very low levels (*SI Appendix*, Fig. S5*B*), which may prevent this mutant from triggering yeast growth. However, the K209E and E74K mutant constructs were stably expressed in yeast (*SI Appendix*, Fig. S5*B*).

SEC-MALS and SEC-SAXS analysis of purified recombinant L6^{TIR} (residues 29–233) revealed an average molecular mass of 38.5 kDa, which is between the expected mass for a monomer (23.4 kDa) and dimer (46.8 kDa) (*SI Appendix*, Table S2 and Fig. S4 *B* and *C*), consistent with previous analysis (9). Substitutions of residues F79 or K209 by alanine or negatively charged residues resulted in a decreased (although slightly larger than monomer) average molecular mass (*SI Appendix*, Table S2 and Fig. S4*B*), consistent with the absence of interaction observed in yeast. The E74K mutant could not be produced recombinantly in *E. coli*. Likewise, mutations in the L6^{TIR} DE interface previously shown to affect L6^{TIR} self-association (9) also led to a decreased (although slightly larger than monomer) average molecular mass in solution (*SI Appendix*, Table S2 and Fig. S4*B*). L6^{TIR} with substitutions in both interfaces, including F79A/R164A and F79A/K200E, had an average molecular mass consistent with monomer (*SI Appendix*, Table S2 and Fig. S4*B*), suggesting that self-association in solution was fully abolished in these double interface mutants. Strikingly, the R164E mutation led to a molecular mass close to a trimer (70.2 kDa) and the F79A/R164E double mutant had an average molecular mass between those expected for dimer and trimer (*SI Appendix*, Table S2 and Fig. S4*C*). These observations suggest that the AE and DE interfaces both contribute to L6^{TIR} self-association in solution and in yeast.

We then tested the effect of the AE- and DE-interface mutations on L6^{TIR} autoactivity, using *Agrobacterium*-mediated

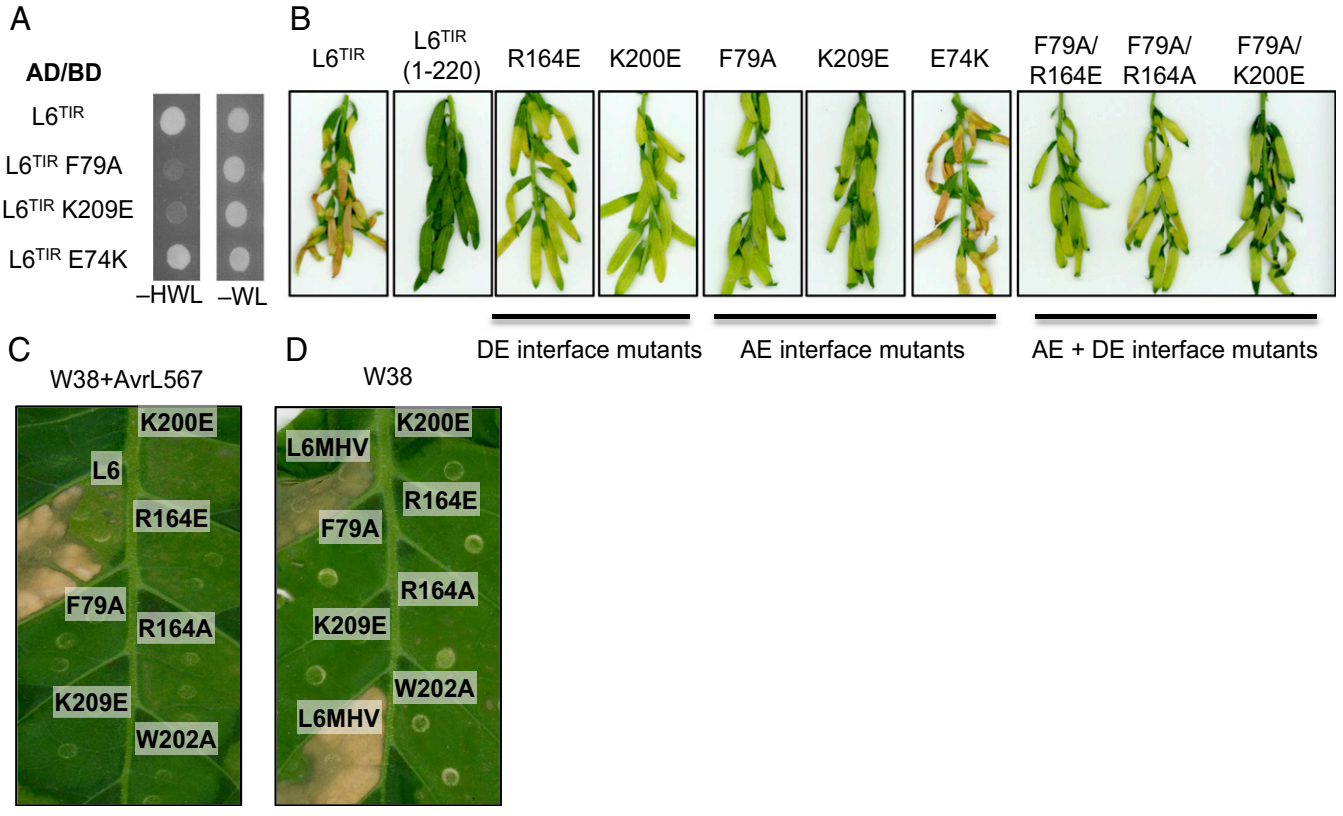

Fig. 3. Mutations in both AE and DE interfaces affect L6^{TIR} self-association and autoactivity and full-length L6 effector-dependent and effector-independent cell-death signaling. (*A*) Mutations in the AE interface disrupt L6^{TIR} self-association in yeast. Growth of yeast cells expressing GAL4-BD and GAL4-AD fusions of L6^{TIR} (residues 29–233) or L6^{TIR} mutants on nonselective media lacking tryptophan and leucine (–WL) or selective media additionally lacking histidine (–HWL). (*B*) Mutations in the AE interface disrupt L6^{TIR} signaling activity in planta. Cell-death signaling activity of L6^{TIR} (residues 1–233) mutants fused to yellow fluorescent protein (YFP), 12 d after agroinfiltration in flax plants. The truncated L6 TIR domain (residues 1–220) was used as a negative control (9). *Agrobacterium* cultures carrying L6^{TIR} mutants were adjusted to OD1. (*C*–*D*) Representative cell-death activity of L6 (*C*) and L6^{MHV} (*D*) mutants, fused to YFP, 3 d after agroinfiltration in wild-type tobacco W38 or transgenic tobacco W38 carrying AvrL567, respectively. *Agrobacterium* cultures carrying L6 and L6^{MHV} mutant were adjusted to OD 0.5.

transient expression in flax. As previously reported (9), mutations in the DE interface such as R164A/E and K200E significantly reduced the L6^{TIR} autoactive phenotype. The F79A and K209E mutations in the AE interface, which affected self-association, also suppressed L6^{TIR} autoactivity, whereas the E74K mutation (which had no effect on self-association in Y2H) did not (Fig. 3*B*). Double mutations in both interfaces, including F79A/R164A, F79A/R164E, and F79A/K200E, resulted in similar phenotypes to the single mutations. All mutants were stably expressed in flax leaves (*SI Appendix*, Fig. S5*C*). These observations suggest that both the AE and DE interfaces contribute to autoactivity of L6^{TIR}; however, neither single nor double mutations completely abolish L6^{TIR} signaling activity.

Both AE and DE Interfaces Are Required for L6 Effector-Dependent and Effector-Independent Signaling Activation. We generated AE- and DE-interface mutants in the full-length L6 protein and tested their effects on effector-dependent and effector-independent cell-death signaling. *Agrobacterium*-mediated transient expression of L6 in transgenic *Nicotiana tabacum* (tobacco) leaves, expressing the corresponding flax-rust (*Melampsora lini*) effector protein AvrL567, induces a strong cell-death response (9) (Fig. 3*C*). Mutations in both the AE (F79A and K209E) and the DE (K200E, R164E, R164A, and W202A) interfaces abolished L6 effector-dependent cell-death signaling (Fig. 3*C*). Immunoblot analysis showed that the K209E construct was not expressed in tobacco, whereas all of the other constructs expressed at a comparable level to the wild-type L6 protein (*SI Appendix*, Fig. S5*D*).

These mutations were also introduced in the autoactive variant of L6, L6^{MHV}, which contains a D-to-V mutation in the MHD motif in the ARC2 subdomain and induces a strong necrotic reaction when transiently expressed in wild-type tobacco W38 without AvrL567 (28). Mutations in both the AE and DE interfaces abolished this autoactive cell-death reaction (Fig. 3*D*), although small cell-death spots were observed with L6^{MHV} R164A mutant. Immunoblotting showed that all mutant proteins were expressed in planta (*SI Appendix*, Fig. S5*E*). Thus, mutations in either AE or DE interfaces suppress L6 effector-dependent and effector-independent cell-death signaling.

Residues in the DE Interface Contribute to RPS4^{TIR} Self-Association and Autoactivity. When overexpressed in planta, RPS4^{TIR} is autoactive and triggers an effector-independent cell-death response (7). RPS4^{TIR} self-associates and can form a heterodimer with RRS1^{TIR} through the AE interface (11). The DE interface is not observed in the crystal structures of RPS4^{TIR}, RRS1^{TIR}, or their heterodimer. To test whether the DE interface could also play a role in RPS4^{TIR} self-association, heterodimerization with RRS1, and autoactivity, we first generated a model of the DE interface in RPS4^{TIR}, by superposition of RPS4^{TIR} onto the L6^{TIR} DE-interface dimer (*SI Appendix*, Fig. S6*B*). The L6 residues R164 and K200 appear to play important roles in stabilizing the DE-interface structure and mutation of either residue suppresses L6^{TIR} self-association and autoactivity (9). Mutation of the equivalent residues in RPS4^{TIR} (R116 or M150), abolished RPS4^{TIR} self-association in Y2H assays (Fig. 4*A*), but did not affect its interaction with RRS1^{TIR} or protein accumulation in yeast (Fig. 4*B* and *SI Appendix*, Fig. S5*F*). The self-association of these RPS4^{TIR} mutants was further examined using SEC-MALS. RPS4^{TIR} (residues 10–178, equivalent to the crystal structure) had an average molecular mass of 21.1 kDa, which is only slightly higher than the expected monomeric mass of 19.6 kDa (*SI Appendix*, Table S2 and Fig. S4*D*). We previously reported a similar in-solution molecular mass of ~23 kDa for RPS4^{TIR} in a slightly different experimental setup (11). The AE-interface mutant S33A, which was previously shown to reduce the RPS4^{TIR} self-association (11), led to an average molecular mass of 19.9 kDa (*SI Appendix*, Table S2). The R116A in the DE interface also resulted in a slight average molecular mass reduction, whereas the M150R mutation was indistinguishable from the wild-type protein (*SI Appendix*, Table S2 and Fig. S4*D*). Although consistent with the DE-interface

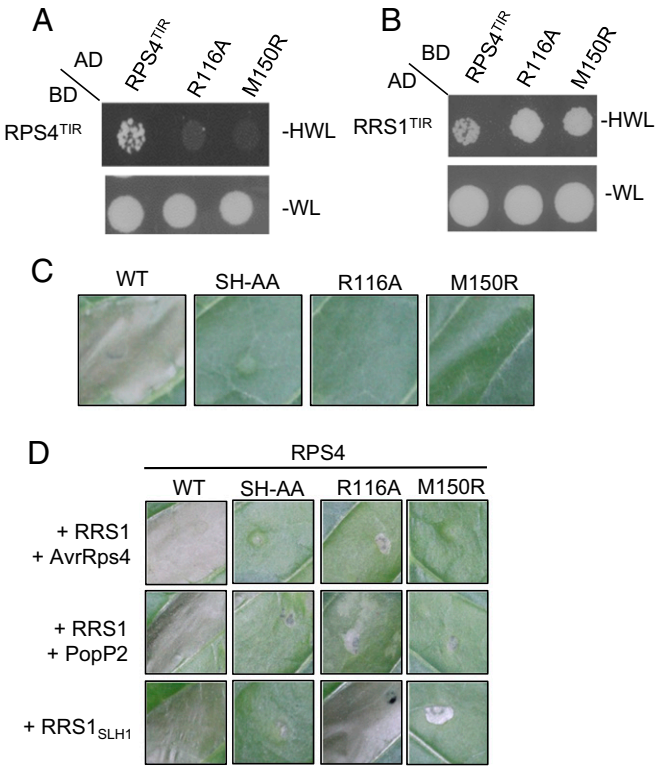

Fig. 4. Mutations in both AE and DE interfaces affect RPS4^{TIR} self-association and autoactivity and full-length RPS4 effector-dependent and effector-independent cell-death signaling. (*A*) Mutations in the DE interface disrupt RPS4^{TIR} self-association in yeast. Growth of yeast cells expressing GAL4-BD fusion and GAL4-AD fusion of RPS4^{TIR} (residues 1–183) or RPS4^{TIR} mutants on nonselective media lacking tryptophan and leucine (–WL) or selective media additionally lacking histidine (–HWL). (*B*) Mutations in the DE interface do not affect RPS4^{TIR} interaction with RRS1^{TIR}. Growth of yeast cells coexpressing GAL4-BD fusion of RPS4^{TIR} or RPS4^{TIR} mutants and GAL4-AD fusion of RRS1^{TIR} (residues 1–185) on –WL or –HWL media. (*C*) Mutations in the DE interface disrupt RPS4^{TIR} signaling activity in planta. Cell-death signaling activity of RPS4^{TIR} (WT, wild-type) and its mutants fused to C-terminal 6xHA tags, 3 d after agroinfiltration in tobacco. (*D*) Representative cell-death activity of full-length RPS4 (WT, wild-type) and its mutants fused to C-terminal 3xHA tags, upon *agro*-mediated transient coexpression with RRS1 and corresponding effectors (AvrRps4 or PopP2), or with RRS1$_{SLH1}$ mutant in W38 tobacco. *Agrobacterium* cultures were adjusted to OD 0.1. Photos were taken 5 d after agroinfiltration.

R116A mutation suppressing RPS4^{TIR} self-association in solution, the low level of self-association of wild-type RPS4^{TIR} detected in this assay and the minor differences observed for the mutants indicate that SEC-MALS may not be sufficiently sensitive to confirm this interaction. Nevertheless, the Y2H data suggest that mutations in both the DE and AE interfaces disrupt RPS4^{TIR} self-association.

We then tested the effect of the DE-interface mutations on RPS4^{TIR} autoactivity. When transiently expressed in tobacco W38, RPS4^{TIR} (residues 1–236) triggered a cell-death response, whereas mutations of the SH motif (SH-AA) in the AE interface as well as either of the R116 and M150 residues in the DE interface abolished this autoactive phenotype (Fig. 4*C*). All mutants were expressed at similar levels to the wild-type RPS4^{TIR} (*SI Appendix*, Fig. S5*G*). These observations suggest that the integrity of both AE and DE interfaces is required for the self-association and autoactivity of RPS4^{TIR}, but the AE interface is the primary interface for RPS4^{TIR} and RRS1^{TIR} heterodimerization.

Both AE and DE Interfaces Are Required for RRS1:RPS4 Effector-Dependent and Effector-Independent Activation. We further examined whether the mutations in the putative DE interface affect effector-dependent activation of the full-length RRS1:RPS4 protein pair. We previously

reported that coexpression of RPS4 and RRS1 with the effectors AvrRps4 or PopP2 in tobacco triggers a strong cell-death response that is abolished by mutations of the SH motif in the AE interface (11). Similarly, mutants in the DE interface also affected RRS1:RPS4 effector-triggered cell death, although the proteins were all expressed (Fig. 4*D* and *SI Appendix*, Fig. S5*H*). The M150R mutant triggered no cell-death response when coexpressed with RRS1 and either effector. Mutation of R116 also disrupted AvrRps4 recognition but induced a weak cell-death response upon PopP2 recognition. To measure the effect of mutations in the DE interface on RPS4 effector-independent signaling, we coexpressed RPS4 mutants with the $RRS1_{SLH1}$ variant, which contains a single amino acid (leucine) insertion in the WRKY domain and activates effector-independent cell death in the presence of RPS4 (11, 29). Mutations of the SH motif in RPS4 abolished cell-death signaling (Fig. 4*D*). The M150R mutant also disrupted RPS4 effector-independent cell death, whereas the R116A mutation did not (Fig. 4*D*). The greater effect of the M150R mutation compared with R116A on full-length RPS4 protein function may be due to its central position in the DE interface, whereas R116 is located at the periphery of the $RPS4^{TIR}$ DE interface. These observations further corroborate that, whereas both interfaces are involved in $RPS4^{TIR}$ self-association and signaling, the AE interface is the primary interface for $RPS4^{TIR}$ and $RRS1^{TIR}$ heterodimerization.

The Crystal Structure of the $RPP1^{TIR}$ Features AE and DE Interfaces. We recently showed that alleles of the *Arabidopsis* NLR protein RPP1 from ecotypes Niederzenz (NdA) and Wassilewskija (WsB) differ in their ability to induce effector-independent cell death via transient expression of the TIR domain in planta (15). RPP1 NdA-1 and WsB alleles differ by 17 substitutions in the TIR domain. Biophysical and functional analyses of proteins where these residues are mutated show a correlation between self-association and the ability for RPP1 TIR domains to induce effector-independent cell death (15). In light of these findings, we undertook structural studies of the RPP1 NdA-1 TIR domain (residues 93–254; $RPP1^{TIR}$). Strikingly, the crystal structure (2.8-Å resolution; *SI Appendix*, Table S1) reveals AE and DE interfaces analogous to $SNC1^{TIR}$ (Fig. 5 *A*–*C* and *SI Appendix*, Fig. S7). Upon superposition of one molecule in the DE-interface dimers, the αE-helix is rotated ∼97° in $RPP1^{TIR}$ compared with its position in $L6^{TIR}$ in the other molecule (Fig. 5*C*). Despite this difference to other TIR domain structures, there are common residues within the AE and DE interfaces of the RPP1 crystal structure (*SI Appendix*, Fig. S7).

Discussion

Structural Conservation of TIR Domain Interfaces in Plants. TIR domains feature in innate immunity pathways across phyla (21); however, the molecular mechanisms of signaling by these domains have largely remained elusive. Whereas in mammalian TIR domains no common trends have emerged among the available crystals structures in terms of protein–protein association (21), most plant TIR-domain crystal structures feature structurally analogous AE interfaces (Figs. 1*B* and 5*B*) (23). The exception is $L6^{TIR}$, the crystal structure of which features the DE but not the AE interface. DE interfaces are also observed in the two structures reported here, of $SNC1^{TIR}$ and $RPP1^{TIR}$, and in the structure of AtTIR (*SI Appendix*, Fig. S8), albeit with some deviations in orientation (Figs. 1*C* and 5*C* and *SI Appendix*, Fig. S9). Whereas the presence or absence of an interface in the crystal does not prove or disprove a biological function (30), these observations precipitated a thorough assessment of interfaces in several proteins, as described here. We conclude that self-association through both the AE and DE interfaces plays a general role in TIR–NLR signaling.

TIR-Domain Self-Association and Signaling Through Conserved TIR Domain Interfaces. We have previously shown that both $L6^{TIR}$ and $RPS4^{TIR}$ signaling requires self-association, focusing on the single dimerization interfaces (DE and AE, respectively) observed in these crystal structures. Here we show that mutations in either of the AE or DE interfaces suppress self-association, effector-dependent immunity, and effector-independent autoactivity in both $L6^{TIR}$ and $RPS4^{TIR}$. In Y2H assays, single mutations to residues in distinct (either the AE or DE) interfaces abolish self-association, suggesting that in this assay, interaction through both interfaces is required for detection. Similarly, mutations of residues in either the AE or DE interfaces can independently abolish cell death. Collectively, these data suggest that self-association through AE and DE interfaces is required simultaneously to allow cell-death signaling by L6 and RPS4.

For $SNC1^{TIR}$, both AE and DE interfaces are observed within the crystal structure. Although only mutations in the AE interface were observed to significantly affect $SNC1^{TIR}$ self-association in solution, mutations in either interface suppressed $SNC1^{TIR}$ cell-death signaling, indicating that the intergrity of both interfaces is required for function. In the case of $RPP1^{TIR}$, several previously identified mutations that affect self-association and cell-death signaling (15) map to either the AE or DE interfaces in the $RPP1^{TIR}$ structure. Therefore, the data presented here and previously (9, 11, 15) suggest a correlation between TIR-domain self-association and cell-death signaling. One exception to this correlation is $RPV1^{TIR}$ from *Mirabilis rotundifolia*; no self-association of this protein could be detected in solution or yeast, but nevertheless, mutations within the predicted AE- and DE-interface regions suppressed its cell-death signaling function (23). All of the TIR:TIR domain interactions studied to date are weak and transient, with the exception of the heterodimer association between $RRS1^{TIR}$ and $RPS4^{TIR}$, which appears to play an inhibitory rather than signaling role. Thus, the failure to detect $RPV1^{TIR}$ self-interaction may be due to the weak self-association of this TIR domain, below the detection threshold limit. The weak and transient nature of TIR:TIR domain interactions may be a key regulatory mechanism to reduce the occurrence of cell-death signaling in the absence of an appropriate stimulus. It is also likely that the TIR-domain self-association is stabilized by other domains in the NLR, by other proteins that promote cell-death

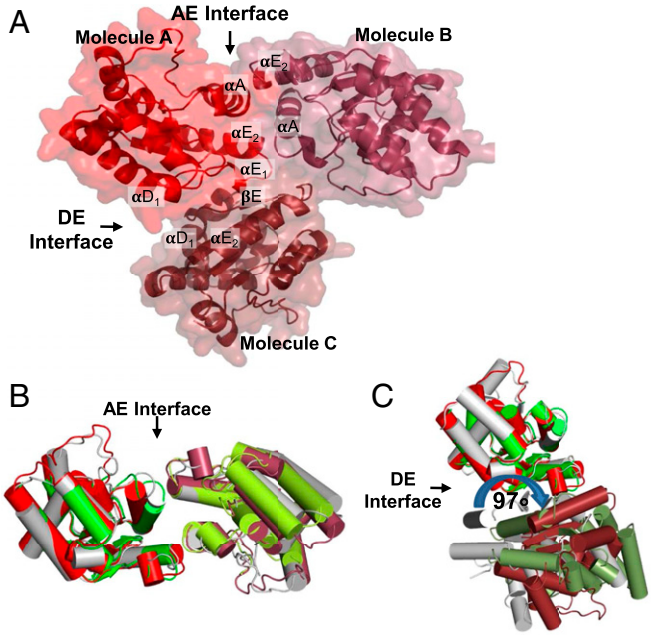

Fig. 5. The AE and DE interface in the crystal structure of $RPP1^{TIR}$. (*A*) Ribbon representation of the RPP1 crystal structure and the AE and DE interfaces, with molecules sharing the AE interface colored red and raspberry and the DE interface, red and ruby. (*B*) Comparison of the AE interface from the $RPS4^{TIR}$ (gray), $SNC1^{TIR}$ (green and lime), and $RPP1^{TIR}$ (red and raspberry) with the chains on the *Left* superimposed, highlighting the strong structural conservation of the interface. (*C*) Comparison of the DE interface from the $L6^{TIR}$ (gray), $SNC1^{TIR}$ (green and forest), and $RPP1^{TIR}$ (red and ruby) structures; only the chains at the *Top* are superimposed, highlighting the rotation observed at the DE interface in these crystal structures.

signaling in planta, or that the TIR domains interact with nonself TIR domains in planta to propagate signaling. Regardless of the exact mechanisms, the required integrity of the AE and DE interfaces suggests that TIR:TIR domain association through both these interfaces is a general requirement for function.

Cooperative Assembly of TIR Domains. Higher-order assembly formation has become an emerging theme in diverse innate immunity pathways. Protein domains from the death-domain family appear to be able to form large, often open-ended helical structures (31). Signaling by cooperative assembly formation (SCAF) explains the ultrasensitive all-or-none response desirable in such pathways (2). One notable feature of the AE and DE interface is that they are not mutually exclusive. In fact, based on the $SNC1^{TIR}$ domain structure, it is possible to build a hypothetical extended TIR domain superhelix propagated through the AE and DE interfaces that are observed in the crystal structure (*SI Appendix*, Fig. S10*A*). An AE interface is also conserved and functional in $L6^{TIR}$; therefore, it is possible for $L6^{TIR}$ to oligomerize through the conserved AE interface and the DE interface observed in the $L6^{TIR}$ crystals. Such an assembly results in a superhelix similar to the one proposed for $SNC1^{TIR}$ (*SI Appendix*, Fig. S10*B*). The same is not possible for $RPP1^{TIR}$, as rotation around the DE interface causes a clash when constructing the hypothetical superhelix (*SI Appendix*, Fig. S10*C*). As such, the varying rotations of different TIR domains suggest there is flexibility in this region, and that a specific geometry is required for TIR domains to form larger oligomeric structures. To date, the only evidence of a TIR-domain self-association complex greater than a dimer was observed in the $L6^{TIR}$ carrying an R164E mutation. The R164E actually suppresses signaling, but the mutant self-associates more strongly in solution compared with wild-type $L6^{TIR}$. Interstingly, the R164A mutation reduces both signaling and self-association, suggesting that the charge substitution mutation at this site may favor an altered specific geometry of association, leading to the formation of an inactive oligomer.

Signaling by Plant TIR Domains in a TIR–NLR Receptor. Ultimately, we need to consider the AE- and DE-interface interactions in the context of a full-length TIR–NLR receptor. Although to date there is no structural data for a full-length receptor, analysis of their mammalian NLR counterparts demonstrates that the nucleotide-binding domain plays a key role in the self-association of the NLRC4 receptor into 10–12 subunit oligomers (18, 19). If plant NLRs follow a nucleated NB-mediated assembly mechanism as observed in animal NLRs (2, 18, 19), this could elegantly induce a proximity-induced assembly of the associated TIR domains through the AE and DE interfaces. Data are starting to emerge on NLR oligomerization upon effector recognition (specifically in tobacco N protein (32) and *Arabidopsis* RPP1 (15)). Many plant TIR domains do not show autoactivity outside the context of the full-length protein (7, 15), suggesting they may not be able to interact adequately on their own without the help from other domains in the NLR.

Materials and Methods

Details of the methods used are provided in *SI Appendix*, *Methods*, including cloning details for vectors and gene constructs, crystallization and structure determination using X-ray crystallography, biophysical experiments including SEC-MALS and SAXS experiments, transient expression in planta, Y2H assays, immunoblot analysis, and ion-leakage measurements.

ACKNOWLEDGMENTS. We thank Stella Césari for discussion and assistance with the in planta immunoprecipitation experiments, Kim Newell for excellent technical support, and Daniel Ericsson for help with X-ray data processing. We acknowledge the use of the University of Queensland Remote Operation Crystallization and X-Ray Diffraction Facility. This research used macromolecular crystallography (MX) and small/wide angle X-ray scattering (SAXS/WAXS) beamlines at the Australian Synchrotron, Victoria, Australia. This research was supported by the Australian Research Council (ARC) Discovery Projects (DP120100685, DP120103558, and DP160102244) and the National Science Foundation (NSF-IOS-1146793 to B.J.S.). B.K. is a National Health and Medical Research Council Research Fellow (1003325 and 1110971). M.B. and S.J.W. are recipients of ARC Discovery Early Career Research Awards (DE130101292 and DE160100893, respectively).

1. Dodds PN, Rathjen JP (2010) Plant immunity: Towards an integrated view of plant-pathogen interactions. *Nat Rev Genet* 11(8):539–548.
2. Bentham A, Burdett H, Anderson PA, Williams SJ, Kobe B (August 24, 2016) Animal NLRs provide structural insights into plant NLR function. *Ann Bot*, 10.1093/aob/mcw171.
3. Duxbury Z, et al. (2016) Pathogen perception by NLRs in plants and animals: Parallel worlds. *BioEssays* 38(8):769–781.
4. van der Biezen EA, Jones JD (1998) The NB-ARC domain: A novel signalling motif shared by plant resistance gene products and regulators of cell death in animals. *Curr Biol* 8(7):R226–R227.
5. McHale L, Tan X, Koehl P, Michelmore RW (2006) Plant NBS-LRR proteins: Adaptable guards. *Genome Biol* 7(4):212.
6. Frost D, et al. (2004) Tobacco transgenic for the flax rust resistance gene L expresses allele-specific activation of defense responses. *Mol Plant Microbe Interact* 17(2):224–232.
7. Swiderski MR, Birker D, Jones JD (2009) The TIR domain of TIR-NB-LRR resistance proteins is a signaling domain involved in cell death induction. *Mol Plant Microbe Interact* 22(2):157–165.
8. Krasileva KV, Dahlbeck D, Staskawicz BJ (2010) Activation of an Arabidopsis resistance protein is specified by the in planta association of its leucine-rich repeat domain with the cognate oomycete effector. *Plant Cell* 22(7):2444–2458.
9. Bernoux M, et al. (2011) Structural and functional analysis of a plant resistance protein TIR domain reveals interfaces for self-association, signaling, and autoregulation. *Cell Host Microbe* 9(3):200–211.
10. Maekawa T, et al. (2011) Coiled-coil domain-dependent homodimerization of intracellular barley immune receptors defines a minimal functional module for triggering cell death. *Cell Host Microbe* 9(3):187–199.
11. Williams SJ, et al. (2014) Structural basis for assembly and function of a heterodimeric plant immune receptor. *Science* 344(6181):299–303.
12. Wang GF, et al. (2015) Molecular and functional analyses of a maize autoactive NB-LRR protein identify precise structural requirements for activity. *PLoS Pathog* 11(2):e1004674.
13. Cesari S, et al. (2016) Cytosolic activation of cell death and stem rust resistance by cereal MLA-family CC-NLR proteins. *Proc Natl Acad Sci USA* 113(36):10204–10209.
14. Kanzaki H, et al. (2012) Arms race co-evolution of Magnaporthe oryzae AVR-Pik and rice Pik genes driven by their physical interactions. *Plant J* 72(6):894–907.
15. Schreiber KJ, Bentham A, Williams SJ, Kobe B, Staskawicz BJ (2016) Multiple domain associations within the Arabidopsis immune receptor RPP1 regulate the activation of programmed cell death. *PLoS Pathog* 12(7):e1005769.
16. Casey LW, et al. (2016) The CC domain structure from the wheat stem rust resistance protein Sr33 challenges paradigms for dimerization in plant NLR proteins. *Proc Natl Acad Sci USA* 113(45):12856–12861.
17. Collier SM, Hamel LP, Moffett P (2011) Cell death mediated by the N-terminal domains of a unique and highly conserved class of NB-LRR protein. *Mol Plant Microbe Interact* 24(8):918–931.
18. Hu Z, et al. (2015) Structural and biochemical basis for induced self-propagation of NLRC4. *Science* 350(6259):399–404.
19. Zhang L, et al. (2015) Cryo-EM structure of the activated NAIP2-NLRC4 inflammasome reveals nucleated polymerization. *Science* 350(6259):404–409.
20. Reubold TF, Wohlgemuth S, Eschenburg S (2011) Crystal structure of full-length Apaf-1: How the death signal is relayed in the mitochondrial pathway of apoptosis. *Structure* 19(8):1074–1083.
21. Ve T, Williams SJ, Kobe B (2015) Structure and function of Toll/interleukin-1 receptor/resistance protein (TIR) domains. *Apoptosis* 20(2):250–261.
22. Chan SL, Mukasa T, Santelli E, Low LY, Pascual J (2010) The crystal structure of a TIR domain from Arabidopsis thaliana reveals a conserved helical region unique to plants. *Protein Sci* 19(1):155–161.
23. Williams SJ, et al. (2016) Structure and function of the TIR domain from the grape NLR protein RPV1. *Front Plant Sci* 7:1850.
24. Hyun KG, Lee Y, Yoon J, Yi H, Song JJ (2016) Crystal structure of Arabidopsis thaliana SNC1 TIR domain. *Biochem Biophys Res Commun* 481(1–2):146–152.
25. Zhang Y, Goritschnig S, Dong X, Li X (2003) A gain-of-function mutation in a plant disease resistance gene leads to constitutive activation of downstream signal transduction pathways in suppressor of npr1-1, constitutive 1. *Plant Cell* 15(11):2636–2646.
26. Botella MA, et al. (1998) Three genes of the Arabidopsis RPP1 complex resistance locus recognize distinct Peronospora parasitica avirulence determinants. *Plant Cell* 10(11):1847–1860.
27. Wan L, et al. (2013) Crystallization and preliminary X-ray diffraction analyses of the TIR domains of three TIR-NB-LRR proteins that are involved in disease resistance in Arabidopsis thaliana. *Acta Crystallogr Sect F Struct Biol Cryst Commun* 69(Pt 11):1275–1280.
28. Bernoux M, et al. (2016) Comparative analysis of the flax immune receptors L6 and L7 suggests an equilibrium-based switch activation model. *Plant Cell* 28(1):146–159.
29. Noutoshi Y, et al. (2005) A single amino acid insertion in the WRKY domain of the Arabidopsis TIR-NBS-LRR-WRKY-type disease resistance protein SLH1 (sensitive to low humidity 1) causes activation of defense responses and hypersensitive cell death. *Plant J* 43(6):873–888.
30. Kobe B, et al. (2008) Crystallography and protein-protein interactions: Biological interfaces and crystal contacts. *Biochem Soc Trans* 36(Pt 6):1438–1441.
31. Wu H (2013) Higher-order assemblies in a new paradigm of signal transduction. *Cell* 153(2):287–292.
32. Mestre P, Baulcombe DC (2006) Elicitor-mediated oligomerization of the tobacco N disease resistance protein. *Plant Cell* 18(2):491–501.
33. Sainsbury F, Thuenemann EC, Lomonossoff GP (2009) pEAQ: Versatile expression vectors for easy and quick transient expression of heterologous proteins in plants. *Plant Biotechnol J* 7(7):682–693.